Universities of Leeds, Sheffield and York
http://eprints.whiterose.ac.uk/

1   **Corrosion of aluminium metal in OPC- and CAC-based cement matrices**

2

3   Hajime Kinoshita[a], Paul Swift[a], Claire Utton[a], Beatriz Carro-Mateo[b], Geraldine

4   Marchand[c], Nick Collier[d] and Neil Milestone[e]

5

6   [a] Department of Materials Science and Engineering, The University of Sheffield,

7   Mappin Street, Sheffield, S1 3JD, UK

8   [b] The Public University of Navarra, C/ Esquíroz, 30 trasera, Pamplona 31007, Spain

9   [c] The National Institute of Applied Sciences (INSA) Lyon, 20 Avenue Albert Einstein

10   69621 Villeurbanne Cedex, France

11   [d] National Nuclear Laboratory, Chadwick House, Birchwood Park, Warrington, WA3

12   6AE, UK

13   [e] Industrial Research Ltd., 69 Gracefield Road, Lower Hutt, 5040, New Zealand

14

15   **Corresponding author:** Hajime Kinoshita

16   E-mail: h.kinoshita@sheffield.ac.uk

17   Tel.: +44-114-222-5930

18   Fax.: +44-114-222-5943

19

22

23 **Abstract**

24

25 Corrosion of aluminium metal in ordinary Portland cement (OPC) based pastes

26 produces hydrogen gas and expansive reaction products causing problems for the

27 encapsulation of aluminium containing nuclear wastes. Although corrosion of

28 aluminium in cements has been long known, the extent of aluminium corrosion in the

29 cement matrices and effects of such reaction on the cement phases are not well

30 established. The present study investigates the corrosion reaction of aluminium in

31 OPC, OPC-blast furnace slag (BFS) and calcium aluminate cement (CAC) based

32 systems. The total amount of aluminium able to corrode in an OPC and 4:1 BFS:OPC

33 system was determined, and the correlation between the amount of calcium hydroxide

34 in the system and the reaction of aluminium obtained. It was also shown that a CAC-

35 based system could offer a potential matrix to incorporate aluminium metal with a

36 further reduction of pH by introduction of phosphate, producing a calcium phosphate

37 cement.

38

1 Introduction

1.1 Reaction of aluminium in cement

Cement can offer economical options for various applications within the nuclear industry, from the structural members of the power plants to the matrices for nuclear waste encapsulation. Cement based systems, typically containing high replacement levels of blast furnace slag (BFS) or pulverised fly ash (PFA), are used to encapsulate a variety of solid and liquid wastes from the nuclear industry [1]. One of the key features of cement systems based on ordinary Portland cement (OPC) is the high alkaline environment (high internal pH) produced in the hardened materials. This is advantageous for the encapsulation of some wastes, such as heavy metals, promoting precipitation [2,3]. OPC-based systems, however, may not be ideal for the incorporation of reactive metals, in particular aluminium containing wastes, as aluminium corrodes in alkaline solutions [4-6]. The process of corrosion above pH 8.5 is considered to be the oxidation of aluminium metal to aluminate ions $Al(OH)_4^-$, through anodic dissolution of the oxide layer (Al_2O_3) formed on the surface of the aluminium metal [5,6]. In the corrosion reaction of aluminium with OPC paste, hydrogen gas is generated which can cause problems to the integrity of cemented waste form and increase porosity, which is undesirable for waste encapsulation [7].

It is generally accepted that lowering the pH of the cementing system and/or reducing available free water will reduce the reaction of aluminium in the cement matrix [7,8]. Setiadi et al. [7] reduced aluminium corrosion by using a 9:1 BFS-OPC system which has a lower pH than neat OPC. Other studies have used alternative cement systems

64   such as calcium sulfoaluminate (CSA) cements [8] or BFS-OPC and PFA-OPC based

65   systems containing excess gypsum ($CaSO_4 \cdot 2H_2O$) or anhydrite ($CaSO_4$) [9].

66   Reduction in aluminium corrosion was observed with large amounts of ettringite

67   being formed in these cases, due to the availability of excess sulphate. The reduction

68   in corrosion was attributed to the reduced amount of free water available for corrosion

69   reactions, due to incorporation of excess water into ettringite, and the reduction of the

70   internal pH of the cement.

71

72   Calcium aluminate cement (CAC) is another alternative cement system. These

73   systems are of interest for aluminium waste encapsulation as they have a lower

74   internal pH (pH=10.5~11.5 [10]) compared with those of OPC-based systems. The

75   reaction between aluminium and CAC has been studied for refractory castables, and

76   some aspects of the reaction e.g. reaction kinetics, effect of temperature and

77   admixture have been reported [11,12]. However, in these studies only small quantities

78   of CAC (2 wt%) were used. With the application of CAC as a matrix for nuclear

79   waste encapsulation in mind, it is of interest to study the corrosion of aluminium in

80   systems with a much higher concentration of CAC. CAC will react with water alone

81   to form a binder of mixed calcium aluminate hydrates. It may also be mixed with a

82   polyphosphate to form a calcium aluminate phosphate cement, through an acid-base

83   reaction [13].

84

85   Although some studies have been performed in this area, key information on the

86   corrosion reaction of aluminium in different cement matrices still remains unclear. In

87   particular, to what extent the aluminium corrosion could occur has yet to be quantified,

88   and the effect of corrosion reactions on cement phases formed. These are particularly

89 important in the OPC-based systems conventionally used in the nuclear industry.

90 Establishing this information will enable the different cementing systems to be ranked

91 and the maximum amount of aluminium-containing waste that may be incorporated

92 estimated. Quantifying these reactions will, therefore, allow a better design of cement

93 matrices for aluminium encapsulation.

94

95 **1.2 Scope of the work**

96

97 In the present study, a series of experiments were undertaken to investigate the

98 corrosion reaction of aluminium powder in OPC-based systems to establish the

99 maximum extent of aluminium corrosion able to occur. In addition, the reaction

100 between small pieces of aluminium plate and CAC-based systems with/out

101 modification by sodium polyphosphate were assessed to establish the suitability of

102 this matrix for reactive metal encapsulation. The extent of aluminium corrosion

103 between the different cement systems is compared.

104

105 **2 Experimental**

106

107 **2.1 OPC-based systems**

108

109 Chemical compositions of raw materials used in the present study are shown in Table

110 1. OPC-based systems containing aluminium powder were produced in the following

111 manner. Between 0 and 7 g of aluminium powder (< 1 mm Φ) was added to the

112 cement matrices, either a neat OPC or a 4:1 BFS-OPC blend as shown in Table 2. The

113 weighed powders were manually mixed in 50 ml plastic containers with water for 5

114   minutes, sealed and cured at room temperature for 21 days. A second set of grout

115   samples were prepared using the same procedure, and the pH of each grout was

116   measured in air using a pH probe (glass electrode) and meter WTW pH315i. Readings

117   were taken for approximately 10 minutes after mixing with water, up until the grout

118   set and the probe could not be inserted.

119

120   **2.2 CAC-based system**

121

122   CAC-based systems, containing small aluminium plates were produced in the

123   following manner. Two cement systems were used as shown in Table 2; a 6:4 PFA-

124   CAC blend and a 6:4 PFA-CAC with polyphosphate system. Firstly CAC (Secar 51

125   from Kerneos UK) and PFA were slowly added into a mixing bowl containing either

126   distilled water or sodium polyphosphate ($(NaPO_3)_n$, Acros Organics) and boric acid

127   (H_3BO_3, 99.5+ %, Fisher Scientific) dissolved in distilled water. Boric acid was used

128   to counter the accelerated setting of CAC caused by sodium polyphosphate [13], and

129   to improve workability. A Kenwood bench-top planetary mixer was used at speed 1

130   (*ca.* 150 rpm) for the initial mixing of 5 minutes, followed by 10 minutes of mixing in

131   a Silverson high shear mixer at 6000 rpm. A portion of mixed cement pastes were

132   cured in a sealed container for 7 days at 20 °C and 95 % R.H. Another portion of

133   cement pastes was poured into a plastic container (50 ml) and an aluminium plate (50

134   mm x 20 mm x 3 mm) immersed in the grout, as shown in Figure 1. Using this set up,

135   the amount of hydrogen gas generated from the reaction of aluminium with the

136   cement matrix was measured by water displacement in a measuring cylinder.

137   Readings were taken at 7 and 28 days of reaction. The pH of the remaining cement

138   slurries was measured every 30 minutes up to 150 minutes, using the same procedure

139 previously outlined. In addition to the CAC-based system samples, a sample of 3:1

140 BFS-OPC system (W/S = 0.35) was also prepared containing aluminium plate for

141 comparison.

142

143 **2.3 Analysis**

144

145 Cured samples were crushed, then immersed into acetone for 7 days to arrest

146 hydration, and subsequently dried under vacuum. Samples were analysed using X-ray

147 diffraction (XRD, Siemens D500 with Cu-Kα radiation ($\lambda = 1.54178$ Å)), a

148 differential scanning calorimetry (DSC, Netzsch DSC404C) and scanning electron

149 microscopy (SEM, JEOL JSM 6400) in backscattered electron (BSE) imaging mode.

150 The XRD and DSC samples were ground and sieved to < 63 µm. DSC measurement

151 was run from room temperature to 800 °C at a heating rate of 10 °C/min under N_2

152 flow. For SEM analysis, samples were prepared by mounting them in epoxy resin,

153 polishing the observation surface to 1/4 μm and carbon coating.

154

155 **3 Results and discussion**

156

157 **3.1 OPC-based systems**

158

159 **3.1.1 Observations**

160

161 Visual examination of the cement samples revealed an increase in volume of both

162 OPC and 4:1 BFS-OPC systems when the amount of aluminium powder was

163 increased. A clear increase in porosity was observed, believed to be due to the

164   generation of hydrogen gas which has been previously reported [8,9]. Backscattered

165   electron images of selected samples obtained during SEM observation are shown in

166   Figure 2. Porosity appeared to become coarser in both in OPC and 4:1 BFS-OPC

167   systems when more aluminium was introduced, indicated in Figure 2b and 2d. The

168   OPC system containing aluminium retained more anhydrous cement particles than the

169   neat OPC system, showing clearly that water was preferentially consumed by the

170   corrosion of aluminium over the hydration of OPC. This is likely to have contributed

171   to the increase in porosity.

172

173   **3.1.2 Phase analysis**

174

175   Figure 3 shows the XRD patterns for OPC with different amounts of aluminium

176   powder. The peaks associated with portlandite ($Ca(OH)_2$), one of the main hydration

177   products of OPC, clearly decreased as the amount of the aluminium was increased.

178   Reflections for unhydrated alite (Ca_3SiO_5) and belite (Ca_2SiO_4) were identified.

179   Gibbsite ($Al(OH)_3$) was identified in the systems containing aluminium and this

180   appears to be the main crystalline phase formed from the reaction of aluminium in

181   OPC. A weak peak observed around 9-12° (2θ) points to the existence of small

182   amount of sulphate related phases such as monosulphate ($Ca_4Al_2(SO_4)(OH)_{12}.6H_2O$).

183   No aluminium was observed in these traces suggesting the majority has been

184   consumed, within the detection limits of the XRD (~5 wt%).

185

186   The XRD patterns for samples containing BFS are shown in Figure 4. The phases

187   identified were portlandite, strätlingite ($Ca_2Al_2SiO_7.8H_2O$), alite, belite and gehlenite

188   ($Ca_2Al_2SiO_7$), a crystalline phase often present in unreacted BFS [7]. Gibbsite was not

189   observed. The XRD patterns for the 4:1 BFS-OPC system suggest that strätlingite is

190   the main crystalline corrosion product of aluminium in this system. Bayerite

191   ($Al(OH)_3$), reported in a similar system after a much longer curing times (180 days)

192   [7], was not identified in the present investigation. The most remarkable feature of the

193   XRD results for the 4:1 BFS-OPC system was clear evidence that aluminium metal

194   was present in the samples with 4.9 and 7.0 wt% of aluminium loading. This suggests

195   that aluminium metal is much less reactive in the 4:1 BFS-OPC system and that the

196   maximum amount of aluminium powder that will corrode in this particular system is

197   less than 4.9 wt%.

198

199   Figure 5 shows the DSC profiles for OPC containing different amounts of aluminium

200   powder. The endothermic peaks up to 200 ^{o}C are considered to indicate the

201   dehydration of calcium silicate hydrate gel (C-S-H) (95-120 ^{o}C), ettringite (125-135

202   ^{o}C) and monosulphate (185-195 ^{o}C) [14]. Although ettringite was not identified by

203   XRD, it is known that its structure can be destroyed rather easily during preparation of

204   XRD samples [8], and hence may not be observed. In the presence of aluminium, the

205   amount of C-S-H appears to have decreased slightly whereas ettringite and

206   monosulphate have increased slightly. In the temperature range of 200-400 ^{o}C, there is

207   a clear endothermic peak around 260 ^{o}C for an amorphous alumina gel [15,16] along

208   with the main dehydroxylation peak of gibbsite at around 280-310 ^{o}C [17,18]. Both of

209   these peaks increase in intensity, with increasing Al content. The amorphous alumina

210   gel appears to be the main reaction product of aluminium corrosion under the

211   conditions used in the present study. As it is amorphous, it was not observed in XRD.

212   The distinctive peak attributed to the dehydroxylation of portlandite at around 450 ^{o}C

213   decreased as the amount of aluminium in the system increased. This is most likely

214   because hydroxide ion (OH⁻) was consumed by the corrosion reaction of aluminium

215   which forms $Al(OH)_4^-$ and gibbsite, along with amorphous alumina gel. A small peak

216   was also observed at 660 ^{o}C, the melting temperature of aluminium metal, suggesting

217   that a small amount of aluminium metal remained unreacted in the system when 7.0

218   wt% of aluminium was added. Again this was not observed using XRD suggesting the

219   level was below the detection limit (~5 wt%) of XRD.

220

221   Figure 6 shows the DSC results for 4:1 BFS-OPC system. The profiles are more

222   moderate due to the smaller amount of OPC in the system. As in the OPC system

223   when aluminium was added, the peak area due to C-S-H slightly decreased with

224   increasing aluminium content, whereas those for ettringite and monosulphate

225   increased slightly. The peak for the dehydroxylation of portlandite decreased as the

226   amount of initial aluminium increased, similarly to the OPC system but on a smaller

227   scale. Endothermic peaks around 260 ^{o}C suggest that in the 4:1 BFS-OPC system,

228   amorphous alumina gel was again the main reaction product of aluminium corrosion

229   under the conditions of the present study. In contrast, the peak attributed to gibbsite

230   observed in the OPC system at around 280-310 ^{o}C was not observed. Instead, the

231   results indicate the existence of strätlingite, with a dehydration peak observed at

232   around 180-220 ^{o}C [19,20], which corresponds to the XRD results. These results

233   suggest that corrosion of aluminium tends to form strätlingite rather than gibbsite in

234   the BFS-OPC system, whilst amorphous alumina gel forms in both systems.

235   Formation of strätlingite in BFS cements with aluminium has been reported in another

236   study [7]. Significantly less $Ca(OH)_2$ was available in the BFS-OPC system

237   (approximately 1/7 of that available in OPC system) based on the peak area of

238    $Ca(OH)_2$ in Figures 5 and 6 with 0 wt% aluminium. It is evident that the extent of the

239   reaction between the cement system and aluminium metal was much less in the BFS-

240   OPC system. A distinct peak at 660 ^{o}C from the melting of aluminium metal was

241   observed and the peaks attributed to reaction products e.g. alumina gel were

242   significantly less intense.

243

244   **3.1.3 Corrosion of aluminium**

245

246   Using the DSC results, the corrosion reaction of aluminium in OPC and 4:1 BFS-OPC

247   systems was further analysed. Figure 7 (a) shows the peak area of the endothermic

248   reaction between 640-670 ^{o}C for each DSC curve, which is attributed to the fusion

249   (melting) of aluminium metal. Therefore, the peak area simply corresponds to the

250   amount of unreacted aluminium metal left in the system. For the 4:1 BFS-OPC system

251   a linear correlation between the peak area and the initial aluminium content added is

252   clearly observed. Linear fitting of the data suggests that unreacted aluminium metal

253   would be observed in a 4:1 BFS-OPC system when over 2.3 wt% powdered

254   aluminium was added. In other words, the amount of aluminium powder that is able to

255   corrode completely in 4:1 BFS-OPC system under these conditions is approximately

256   2.3 wt%. The gradient of the liner fit, 1.4 J/g, represents the energy required to melt 1

257   wt% of aluminium per unit sample. Thus, the same linear gradient can be applied to

258   the OPC system, where only one point for fusion of aluminium was obtained. This

259   estimates the amount of aluminium able to corrode in neat OPC as approximately 6.0

260   wt% under the conditions of the present study.

261

262   Figure 7 (b) shows similar analysis for the endothermic peak between 405-480 ^{o}C

263   attributed to the dehydroxylation of $Ca(OH)_2$. The peak area is proportional to the

264   amount of $Ca(OH)_2$ presented in the system. The data indicate that the amount of

265    $Ca(OH)_2$ remaining in both systems decreased with increasing aluminium content,

266   more than would be expected from simple dilution due to aluminium additions alone.

267   This reduction of $Ca(OH)_2$ continued and corresponded to the amount of aluminium

268   corroded in the system. Little $Ca(OH)_2$ was observed in the systems where the

269   maximum corrosion of aluminium took place and excess aluminium metal was left

270   unreacted. This suggests that the corrosion of aluminium consumes OH^- and water in

271   the system, and that the level of OH^- becomes too low to sustain the sufficient

272   formation of $Ca(OH)_2$ and further corrosion of aluminium. A significant effect of pH

273   in alkaline solution on the long-term aluminium corrosion (up to 80 days) has been

274   reported [21], and the results obtained in the present study show that this is also the

275   case for the aluminium corrosion in the cementitious matrices.

276

277   The availability of water in the system may also explain the drop in $Ca(OH)_2$ content.

278   A greater amount of unhydrated cement clinker phases remained in the cements with

279   aluminium as observed in the SEM results due to consumption of water in corrosion

280   reactions at the expense of some cement hydration reactions. Consequently less

281    $Ca(OH)_2$ may be expected to have formed. However, this cannot solely be the reason

282   for the suppression of $Ca(OH)_2$ formation, as a significant amount of C-S-H existed in

283   aluminium containing systems as shown in Figures 5 and 6. Therefore, it is reasonable

284   to consider that the consumption of OH^- ions due to the corrosion of aluminium was

285   the main reason for the reduction of $Ca(OH)_2$ in the studied system. The reaction of

286   aluminium with the cement pore solution removes OH^- from solution, reducing the pH.

287   This in turn causes any $Ca(OH)_2$ in the system to dissolve. It is known that $Ca(OH)_2$

288   releases OH^- at pH < 12.4 whereas C-S-H is able to remain stable as low as pH = 11.0

289   ~ 10.5 by changing the Ca/Si ratio through incongruent dissolution [3].

290

291   The gradient of the liner fit in Figure 7 (b), -15.0 J/g, represents the reduction in the

292   energy needed to dehydroxylate $Ca(OH)_2$ in the system, thus the reduction in the

293   amount of $Ca(OH)_2$ through reaction with 1 wt% of aluminium per unit sample. The

294   data for the OPC system suggests that little $Ca(OH)_2$ should be observed in the system

295   when aluminium content exceeds 5.3 wt%. Since 6.0 wt% of aluminium is estimated

296   to corrode in this systems as discussed previously, there must be a small amount of

297   OH^- provided from other phases. In the BFS-OPC system, little $Ca(OH)_2$ would be

298   produced beyond 0.8 wt% of aluminium content when $Ca(OH)_2$ is assumed to be the

299   only source of OH^- as in the OPC system. However, the amount of aluminium

300   estimated to corrode in this systems is 2.3 wt% (Figure 7 (a)). This gap indicates that

301   the assumption is not correct and that a significant amount of OH^- was provided also

302   from other phases. In the BFS:OPC system this is possibly from dissolution of C-S-H.

303   Further studies are required to understand the role of C-S-H in the corrosion of

304   aluminium. It is important to study the corrosion of aluminium over the longer-term

305   as different hydration products may provide OH^- resulting in different corrosion

306   products at various stages of cement hydration. These results also explain why

307   bayerite $(Al(OH)_3)$ formation has been observed in the BFS-OPC system after 180

308   days [7], which was probably due to the slow formation of $Ca(OH)_2$ in the BFS-OPC

309   system.

310

311   **3.1.4 Initial pH of cement pastes**

312

313   Fig. 8 (a) and (b) show the pH of samples at the initial stage of hydration for the OPC

314 and BFS-OPC systems, respectively, with different aluminium contents. As shown in

315 the figures, both for the OPC and 4:1 BFS-OPC systems, the pH of the aluminium-

316 containing samples decreased with time. The decrease occurred more rapidly the more

317 aluminium was added, indicating the increased consumption of hydroxide ions due to

318 aluminium corrosion, which is consistent with the DSC results. Because the BFS-

319 OPC system had a lower pH due to the less OPC and greater effective water volume,

320 the impact of incorporated aluminium on the pH appeared to be greater than in the

321 neat OPC system. The BFS:OPC samples lost their fluidity faster, and the pH

322 decreased more rapidly, however in the longer term the overall amount of corrosion

323 was less. The drop occurs more rapidly in the BFS:OPC samples, due to the overall

324 lower amount of OH- ions available compared to the neat OPC samples, where OH- is

325 more abundant and replenished during OPC hydration.

326

327 **3.2 CAC-based system**

328

329 **3.2.1 Phase analysis**

330

331 Figure 9 shows the XRD patterns of the PFA-CAC system after 7 days of curing at 20

332 ^{o}C with and without the addition of sodium polyphosphate and boric acid. For the 6:4

333 PFA-CAC system, the peaks observed can be attributed to the crystalline phases

334 usually found in hydrated CAC systems i.e., Gibbsite, CAH_{10} ($CaAl_2O_{14}H_{10}$), C_2AH_8

335 ($Ca_2Al_2O_{13}H_{16}$) along with the crystalline phases from the original unhydrated CAC

336 i.e., monocalcium aluminate ($CaAl_2O_4$), gehlenite ($Ca_2Al_2SiO_7$) and perovskite

337 ($CaTiO_3$) or PFA i.e., quartz (SiO_2) and mullite ($Al_6Si_2O_{13}$). Some of the peaks at

338 lower angles may be attributed to a strätlingite-related phase ($Ca_2Al_2SiO_7.7.25H_2O$) or

339   a monosulphate-related phase ($Ca_4Al_2(SO_4)(OH)_{12}.10H_2O$). Formation of such phases

340   related to strätlingite and monosulphate has been reported in a similar system based

341   on PFA-CAC in presence of additional calcium sulphate [22] although this system

342   also formed additional phases ettringite and C_3AH_6 ($Ca_3Al_2(OH)_{12}$). The difference

343   from the present study is probably due to the presence of calcium sulphate.

344

345   When sodium polyphosphate and boric acid were introduced to the 6:4 PFA-CAC

346   system, the XRD results changed significantly. No peaks for the crystalline hydrate

347   phases were observed, with only those from the raw materials were identified. This

348   lack of crystalline CAC hydration products was one of the key features of the sodium

349   polyphosphate modified CAC system in our previous studies [13]. It has been

350   reported that amorphous phases are obtained from CAC with sodium polyphosphate

351   addition [23-25]. Some suggests an amorphous calcium aluminate phosphate hydrate

352   (C-A-P-H) gel [23] while other suggests a mixture of calcium phosphate based gel

353   ($NaCaPO_4.xH_2O$) and alumina gel ($Al_2O_3.xH_2O$) [24]. Because of the compositional

354   flexibility, a generic chemical formula of $Ca_xH_y(PO_4)_z.nH_2O$ has been suggested more

355   recently [25].

356

357   **3.2.2 Initial pH of cement pastes**

358

359   Figure 10 shows the pH of CAC-based cement systems at the initial stages of

360   hydration along with that of the 3:1 BFS-OPC system. The pH of the 3:1 BFS-OPC

361   system (75 wt% BFS) was very similar to that for the 4:1 BFS:OPC (80 wt% BFS)

362   system shown in Figure 8 (b), approximately 13 throughout the measured period. The

363   difference in BFS content appears to have little effect on the pH of BFS-OPC system

364   at this early stage of hydration. On the other hand, the PFA-CAC system exhibited a

365   significantly lower pH level, starting from an initial pH 11.7 rising to 12.1 prior to

366   initial set. When sodium polyphosphate and boric acid were introduced into the PFA-

367   CAC system, there was a dramatic decrease in pH, indicating the effect of acid-base

368   reaction between polyphosphate (acid) and CAC (base) [24]. The pH for this system

369   remained lower (pH 10.3) during the measuring period of 150 minutes. This system

370   may have significantly reduced aluminium corrosion.

371

372   **3.2.3 Corrosion of aluminium**

373

374   In all systems, the generation of hydrogen gas was observed, although the aluminium

375   plates immersed in the cement matrix did not completely corrode after 28 days of

376   reaction. Table 3 shows the amount of the generated hydrogen gas measured after 7

377   and 28 days for each system. The 3:1 BFS-OPC system clearly produced a significant

378   amount of hydrogen gas with the majority generated within the first 7 days. The

379   hydrogen gas release rate was 2.07 ml/cm^2/day in the initial 7 days, and the rate

380   reduced to 0.02 ml/cm^2/day between 7 and 28 days. This reduction is most likely to be

381   caused by the OH$^-$ depletion in the local environment surrounding the aluminium

382   plate due to the initial intensive corrosion reaction of aluminium. As discussed in the

383   former sections, the reaction of aluminium in the OPC-based system will cause a

384   reduction of OH$^-$ and Ca(OH)$_2$ in the system, to the level where no further reaction

385   can occur.

386

387   The PFA-CAC system produced much smaller amounts of hydrogen gas compared to

388   the 3:1 BFS-OPC system. Since the pH of the paste at initial set was lower in the

389   PFA-CAC system, it is expected to have a lower level of internal pH (a lower

390   concentration of OH^-) in the hardened sample compared with the 3:1 BFS-OPC

391   system, which must have contributed to these results. In the PFA-CAC system,

392   however, the generation rate of hydrogen gas did not decrease after 7 days, but

393   slightly increased from 0.14 ml/cm^2/day in the initial 7 days to 0.20 ml/cm^2/day in the

394   following period. These results suggest that the reaction mechanism of aluminium in

395   the PFA-CAC system is different from that in the OPC-based system. It would appear

396   that the OH^- in the PFA-CAC system remained sufficiently high for aluminium

397   corrosion, even after a certain amount of aluminium had reacted. This is most likely

398   due to the conversion reactions of the metastable phases CAH_{10} and C_2AH_8 which

399   inevitably convert to C_3AH_6 and $Al(OH)_3$ as shown in Eqs. 1 and 2 [26].

400

401     $2CAH_{10} \rightarrow C_2AH_8 + 2Al(OH)_3 + 9H_2O$ ----- (1)

402     $3C_2AH_8 \rightarrow 2C_3AH_6 + 2Al(OH)_3 + 9H_2O$ ----- (2)
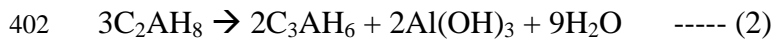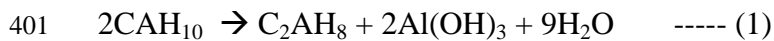
403

404   Although the pH change during these conversion reactions is considered to be

405   minimal [26], they lead to a release of water, which is then available for further

406   reaction of the remaining anhydrous material. It has been suggested that the amount of

407   aluminium corrosion in a CAC-based system corresponds to the extent of the cement

408   hydration reaction [12].

409

410   When sodium polyphosphate and boric acid were introduced into the PFA-CAC

411   system, the generation of hydrogen gas was further reduced, with a release rate as

412   small as 0.02 ml/cm^2/day which did not change throughout the measured period. This

413   must be attributed to the obvious fact that the CAH_{10} and C_2AH_8 phases did not form

414 in this system so the conversion reactions of these phases could not take place

415 releasing water for further hydration reaction of the system. The results also show

416 that aluminium corrosion in the PFA-CAC system can be effectively reduced by

417 adding polyphosphate and boric acid. Further longer term tests are required to

418 establish the extent of hydrogen generation since the present investigation concerns

419 the initial stage of hydration up to 7 days. As discussed in the previous sections,

420 different hydration products would provide OH^- for the corrosion of aluminium

421 resulting in different corrosion products at different stages of cement hydration. This

422 is especially important for the PFA-CAC systems as the conversion of metastable

423 phases appeared to have significant effects on the aluminium corrosion.

424

425 **4 Summary**

426

427 A series of experiments have investigated the reaction of aluminium metal in OPC-

428 and CAC-based systems. The results show that the maximum amount of aluminium

429 powder able to corrode in the neat OPC system investigated in the present study was 6

430 wt%. The amount of hydroxide ion in the system appeared to determine the extent of

431 aluminium corrosion, mainly through $Ca(OH)_2$ in the OPC system. It was found that

432 the corrosion of aluminium could cause the severe reduction of $Ca(OH)_2$ in the system.

433 The corrosion of aluminium was reduced to 2.3 wt% in the 4:1 BFS-OPC system, due

434 to the reduced concentration of OH^- by dilution of OPC and increased effective water

435 volume.

436

437 In the CAC-based system, less initial reaction occurred on the aluminium plate

438 compared with that in the OPC-based system due to the lower matrix pH. However,

439   aluminium continued to corrode slowly in the PFA-CAC system up to 28 days, the

440   maximum time period tested in the present work. Introducing sodium polyphosphate

441   and boric acid provided an effective way to reduce the reaction of aluminium in the

442   PFA-CAC system. The initial pH of the fluid paste at initial set was reduced, and the

443   formations of metastable calcium aluminate hydrates were avoided by forming an

444   amorphous binding phases. This system generated the lowest hydrogen gas release

445   compared with the CAC-PFA based systems and the 3:1 BFS:OPC system. Further

446   long term tests need to be conducted to establish whether calcium aluminate

447   phosphate cements are suitable for long term aluminium encapsulation.

448

449 **Acknowledgement**

450

454

455 **REFERENCES**

456

457 [1] N. B. Milestone, Reactions in cement encapsulated nuclear wastes: need for

458 toolbox of different cement types, Advances in Applied Ceramics, 105 [1] (2006), pp.

459 13-20.

460 [2] F. P. Glasser, Chemistry of cement-solidified waste forms, in: R. D. Spence (Eds.),

461 Chemistry and Microstructure of Solidified Waste Forms, Lewis Publisher, USA

462 (1993) pp. 1-39.

463 [3] M. Atkins, F. P. Glasser, Application of Portland cement-based materials to

464 radioactive waste immobilisation, Waste Management, 12, (1992) pp. 105-131.

465 [4] M. R. Tabrizi, S. B. Lyon, G. E. Thompson, J. M. Ferguson, The long-term

466 corrosion of aluminium in alkaline media, Corrosion Science, 32 (1991) pp. 733-742.

467 [5] R. D. Armstrong, V. J. Braham, The mechanism of aluminium corrosion in

468 alkaline solutions, Corrosion Science, 38 [9] (1996) pp. 1463-1471.

469 [6] S. -M. Moon, S. -I. Pyun, The corrosion of pure aluminium during cathodic

470 polarization in aqueous solutions, Corrosion Science, 39 [2] (1997) pp. 399-408.

471 [7] A. Setiadi, N. B. Milestone, J. Hill, M Hayes, Corrosion of aluminium and

472 magnesium in BFS composite cements, Advances in Applied Ceramics, 105 [4]

473 (2006) pp.191-196.

474 [8] Q. Zhou, N. B. Milestone, M. Hayes, An alternative to Portland Cement for waste

475 encapsulation - The calcium sulfoaluminate cement system, J. Hazard. Mater., 136 [1]

476 (2006) pp. 120-129.

477 [9] N. C. Collier, N. B. Milestone, P. D. Swift, Immobilisation matrices for

478 intermediate level nuclear wastes using sulphate activated BFS/OPC and PFA/OPC

479 composite cements, Advances in Applied Ceramics, 109 [5] (2010) pp. 269-274.

480 [10] Safety data sheet, Secar Range, SDS-Secar-GB062009, Kerneos SA (2008).

481 [11] M. D. M. Innocentini, L. A. Nascimento, A. E. M. Paiva, V. C. Pandolfelli, B. A.

482 Menegazzo, L. R. M. Bittencourt, Aluminium-containing refractory castables, Part I,

483 Evaluation of hydrogen-gas generation, Am. Ceram. Soc. Bull., 82 [6] (2003) pp. 45-

484 51.

485 [12] A. R. Studart, M. D. M. Innocentini, I. R. Oliveira, V. C. Pandolfelli, Reaction of

486 aluminium powder with water in cement containing refractory castables, J. Euro.

487 Ceram. Soc., 25 (2005) pp. 3135-3143.

488 [13] P. Swift, H. Kinoshita, N. C. Collier, C. A. Utton, Phosphate-modified calcium

aluminate cement for radioactive waste encapsulation, Advances in Applied Ceramics, 112 [1] (2013) pp. 1-8.

[14] P. R. Ellis, Analysis of mortars (to include historic mortars) by differential thermal analysis, in: Historic Mortars, Characteristics and Tests, Proceedings, RILEM Publications (2000) pp. 133-147.

 [15] T. Meher, A.K. Basu, S. Ghatak, Physicochemical characteristics of alumina gel in hydroxyhydrogel and normal form, Ceramics International, 31 (2005) pp. 831-838.

[16] J. L. Szetu, R. L. Frost, J. T. Kloprogge, S. C. Russell, W. Martens, Dehydration and dehydroxylation of alumina gels prepared from tri-sec-butoxyaluminium modified with short chain aliphatic acids, Thermochimica Acta, 362 (2000) pp. 37-48.

[17] J. T. Kloprogge, H. D. Ruan, R. L. Frost, Thermal decomposition of bauxite minerals: infrared emission spectroscopy of gibbsite, boehmite and diaspore, J. Mater. Sci., 37 (2002) pp. 1121-1129.

[18] B. Zhu, B. Fang, X. Li, Dehydration reactions and kinetic parameters of gibbsite, Ceramics International, 36 (2010) pp. 2493-2498.

[19] A. Bakolas, E. Aggelakopoulou, A. Moropoulou S. Anagnostopoulou, Evaluation of pozzolanic activity and physicomechanical characteristics in metakaolin-lime pastes, Journal of Thermal Analysis and Calorimetry, 84 (2006) pp. 157–163.

[20] T. Matschei, B. Lothenbach, F. P. Glasser, Thermodynamic properties of Portland cement hydrates in the system $CaO–Al_2O_3–SiO_2–CaSO_4–CaCO_3–H_2O$, Cement and Concrete Research, 37 (2007) pp. 1379-1410.

[21] M. R. Tabrizi, S. B. Lyon, G. E. Thompson, J. M. Ferguson, The long-term corrosion of aluminium in alkaline media, Corrosion Science, 32 [7] (1991) pp. 733-742.

[22] L. Fernández-Carrasco, E. Vázquez, Reactions of fly ash with calcium aluminate

514   cement and calcium sulphate, Fuel, 88 (2009) pp. 1533-1538.

515   [23] W. Ma, P. W. Brown, Hydration of sodium phosphate-modified high alumina

516   cement, J. Mater. Res., 9 [5] (1994) pp. 1291-1297.

517   [24] T. Sugama, N.R. Carciello, Sodium phosphate-derived calcium phosphate

518   cements, Cement and Concrete Research, 25 [1] (1995) pp. 91-10.

519   [25] S. V. Dorozhkin, Amorphous calcium (ortho)phosphates, Acta Biomaterialia, 6

520   (2010) pp. 4457-4475.

521   [26] K. L. Scrivener, J.-L. Cabiron, R. Letourneux, High-performance concretes from

522   calcium aluminate cements, Cement and Concrete Research, 29 (1999) pp. 1215-1223.

523

524   Table 1 Chemical composition of raw materials.

	OPC (wt%)	BFS (wt%)	CAC (wt%)	PFA (wt%)		Al (wt%)
SiO_2	21.0	34.5	5.04	49.53	Al	>99.63
Al_2O_3	5.2	13.8	51.1	26.45	Cu	0.0019
CaO	64.6	42.1	36.8	1.62	Fe	0.1287
Fe_2O_3	2.6	1.0	1.98	8.70	Mn	0.0030
Na_2O	0.3	0.2	0.11	<0.01	Ti	0.0017
K_2O	0.6	0.5	0.42	4.58	V	0.0052
MgO	2.1	7.3	0.48	1.56	Zn	0.0208
SO_3	2.5	[a]	0.02^{b}	0.88	B	0.0005
TiO_2	-	-	2.08	-	Ga	0.0078
P_2O_5	-	-	0.13	-	Si	<0.10
Chloride	0.05	0.02	-	-	Others	<0.10
Insolubles	0.3	-	-	-		
LOI	0.7	1.0	-	4.10		
Free lime	0.8	-	-	-		
Sulphide	-	0.9	-	-		

[a] Contains reduced sulphur
[b] Determined using Leco analysis

525

526

527   Table 2 Formulation of samples, normalised by the weight of base cement

528   (OPC+BFS=100, CAC+PFA=100).

OPC based system	OPC (wt%)	BFS (wt%)	Water (wt%)			Al powder (wt%)
	100	0	35			0, 2.4, 4.9, 7.0
	20	80	35			
CAC based system	CAC (wt%)	PFA (wt%)	Water (wt%)	Phosphate (wt%)	Boric acid (wt%)	Al plate
	40	60	35	0	0	50x20x3 (mm)
	40	60	35	16	1.2	

529

530

531   Table 3 Hydrogen gas generated from the reaction of aluminium.

	H$_2$ gas generated		Release rate	
	7 days (ml/cm^2)	28 days (ml/cm^2)	0~7 days (ml/cm^2/day)	7~28 days (ml/cm^2/day)
BFS-OPC [a]	14.5	14.8	2.07	0.02
PFA-CAC [b]	1.0	5.2	0.14	0.20
PFA-CAC +Phosphate +Boric acid [b]	0.2	0.5	0.02	0.02

[a] BFS:OPC=3:1, w/s=0.35, [b] See Table 2 for details of formulations

532

533

Plastic container

Cement matrix

Measuring cylinder

Water

Glass vessel

Al
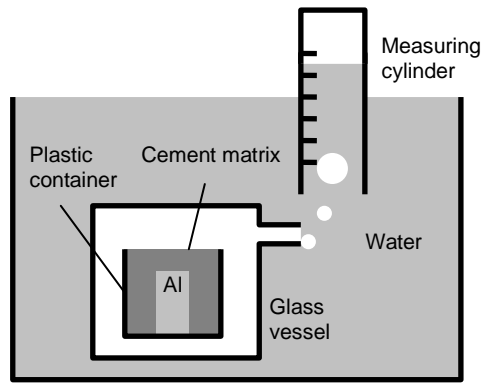
534

535   Fig. 1 Schematic diagram of experimental setup for hydrogen measurement.

536

537

538
539
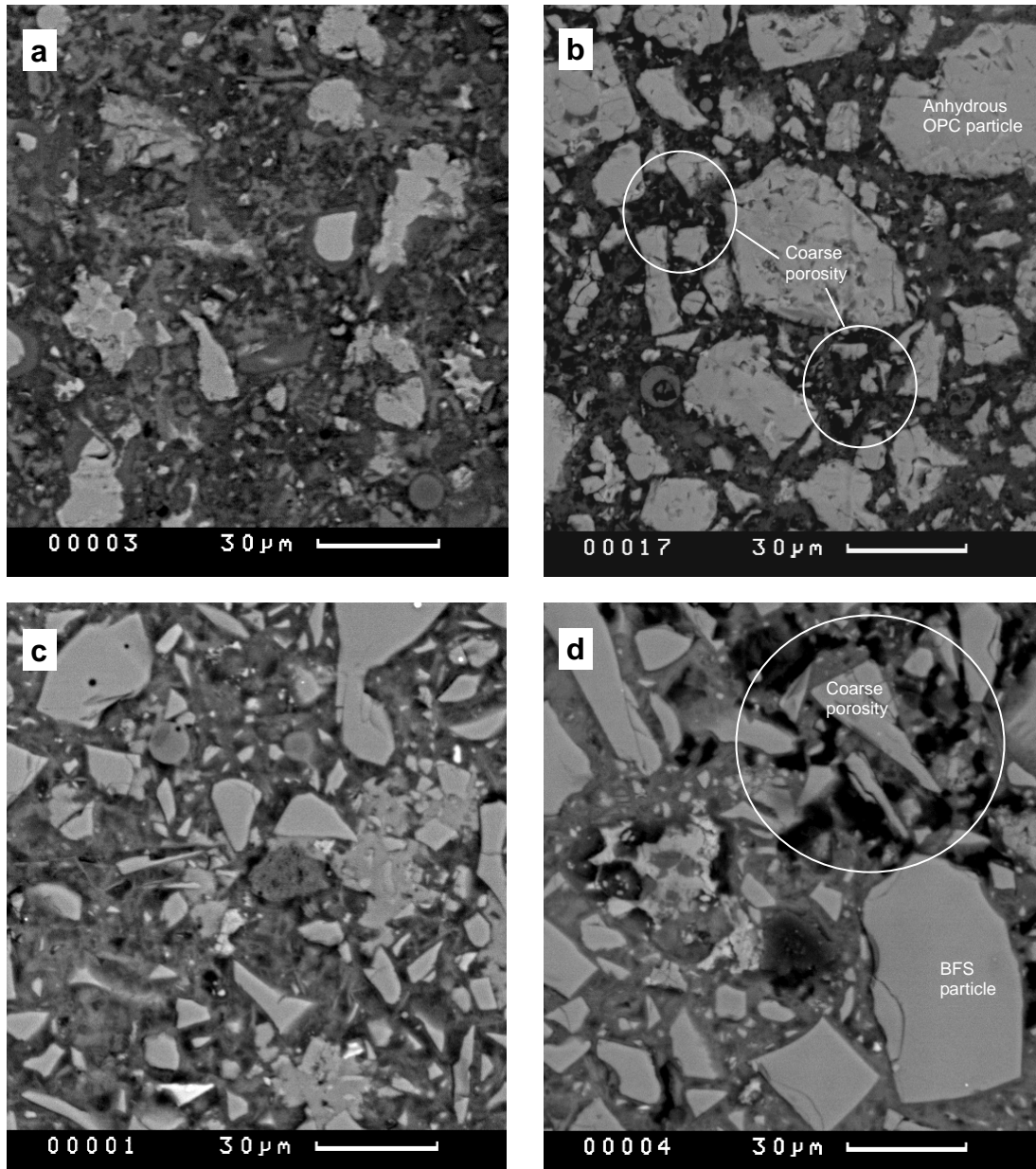
Fig. 2 Backscattered electron images of samples: (a) pure OPC, (b) OPC with 7.0 wt%
of Al, (c) 4:1 BFS-OPC and (d) 4:1 BFS-OPC with 7.0 wt% of Al.

542
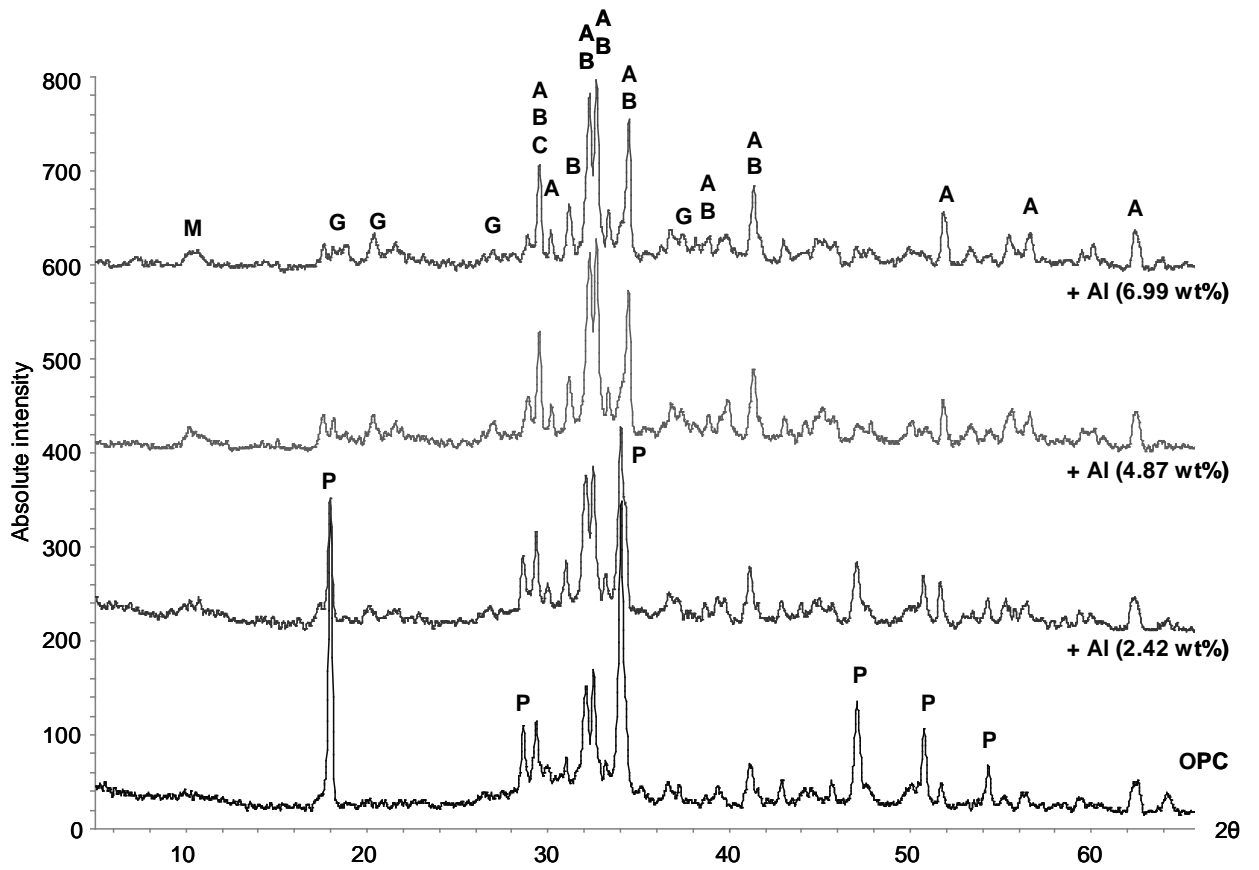
543

544

545   Fig. 3 XRD patterns of OPC system with different amount of aluminium contents

546   after 21 days of curing at room temperature. Reflection peaks are indexed as: A (Alite),

547   B (Belite), C (Calcite), G (Gibbsite), M (Monosulphate), P (Portlandite).

548

549

550
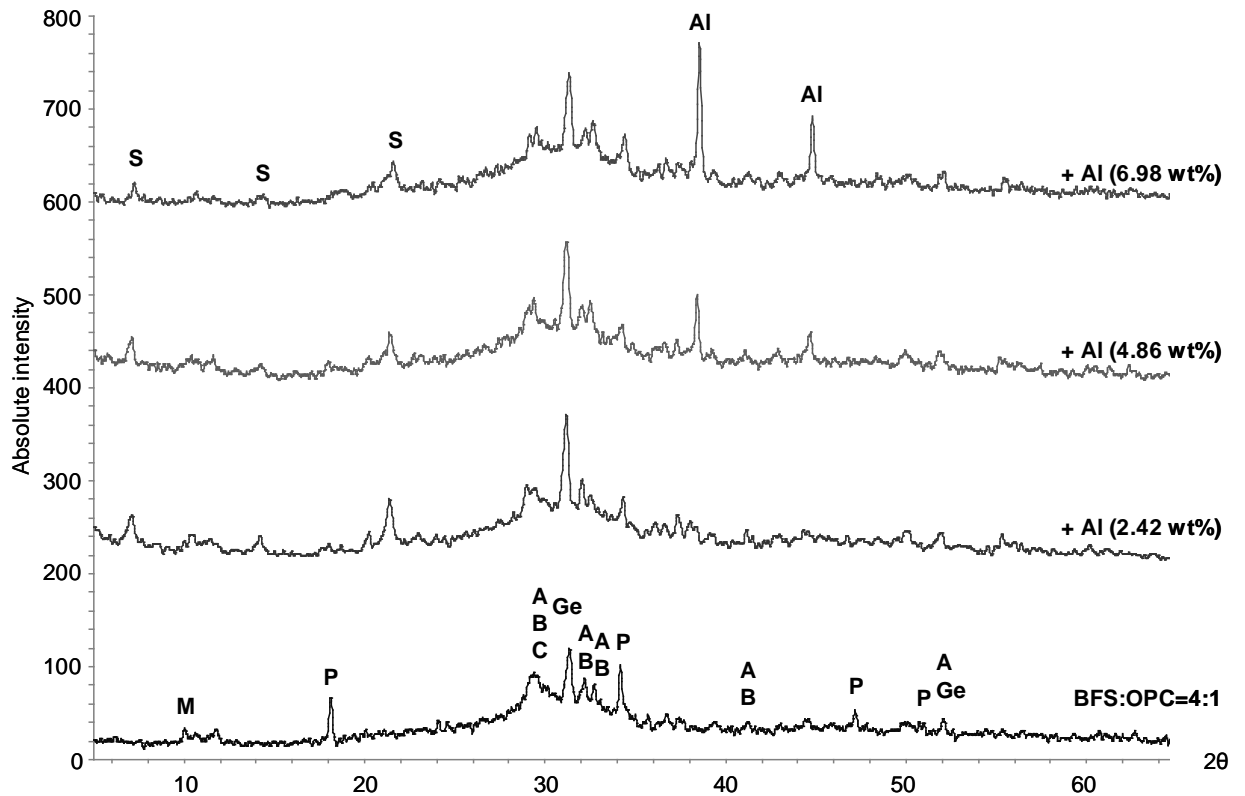
Fig. 4 XRD patterns of 4:1 BFS-OPC system with different amount of aluminium

contents after 21 days of curing at room temperature: Reflection peaks are indexed as:

A (Alite), Al (Aluminium), B (Belite), C (Calcite), Ge (Gehlenite), M (Monosulphate),

P (Portlandite), S (Strätlingite).

555

556

557
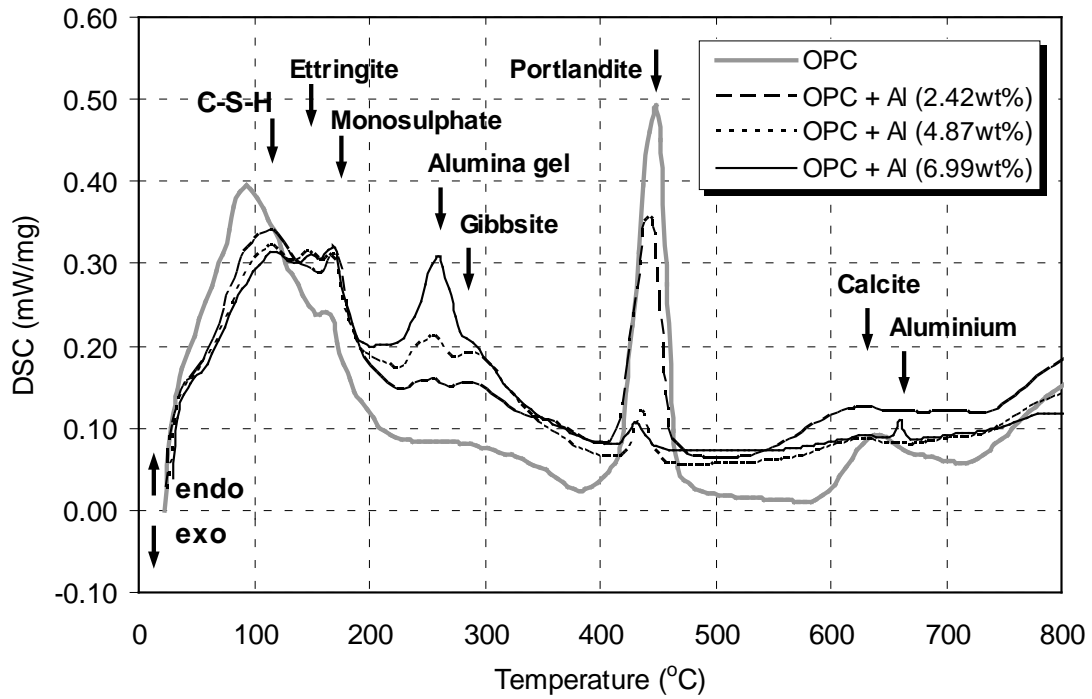
Fig. 5 DSC profiles for OPC system with different amount of aluminium powder after

21 days of curing at room temperature.

560

561
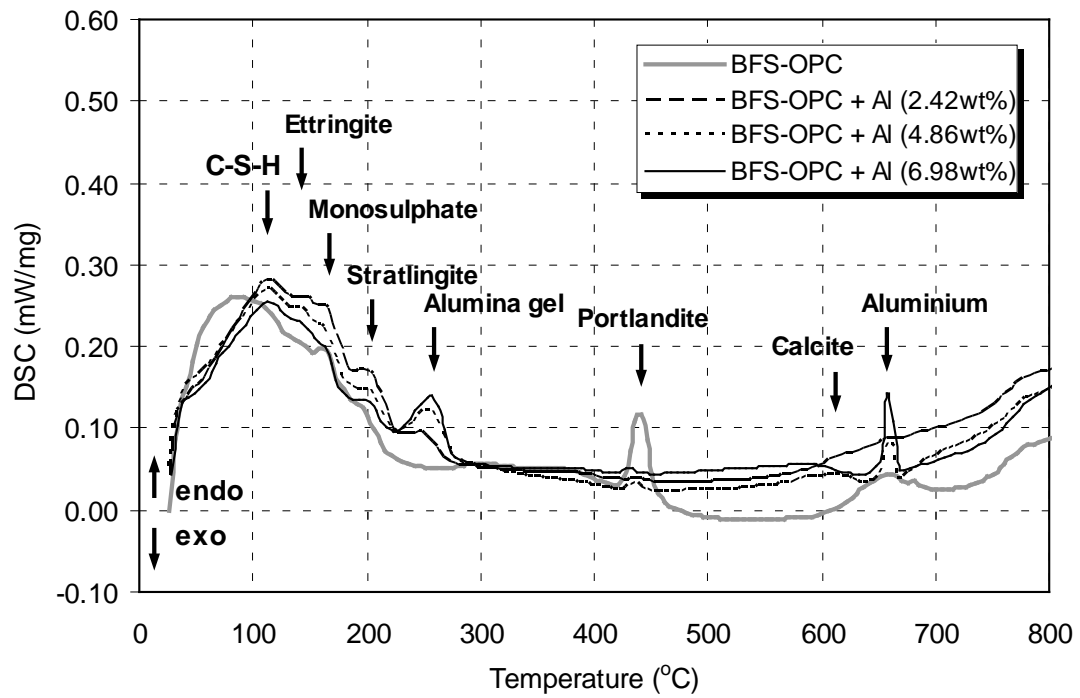
562

563   Fig. 6 DSC profiles for 4:1 BFS-OPC system with different amount of aluminium

564   contents after 21 days of curing at room temperature.
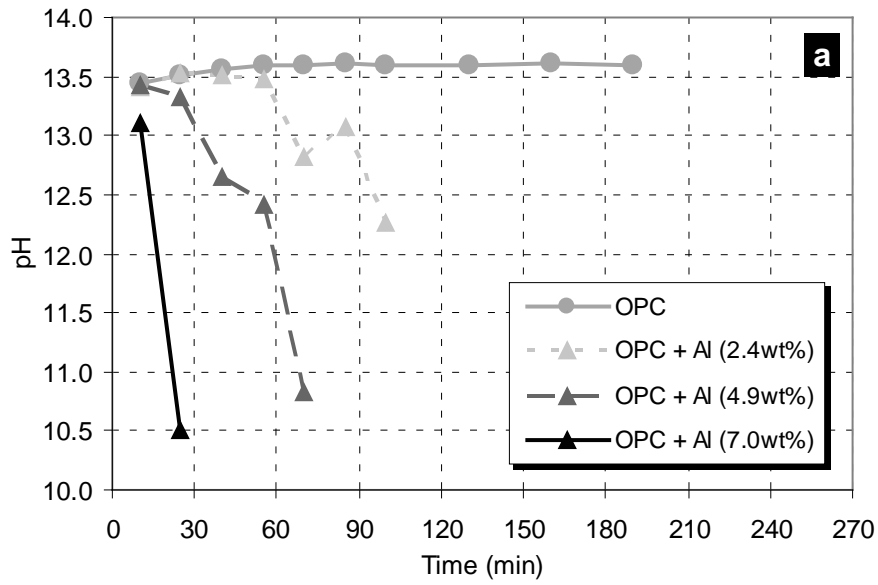
565

566

567

568

569
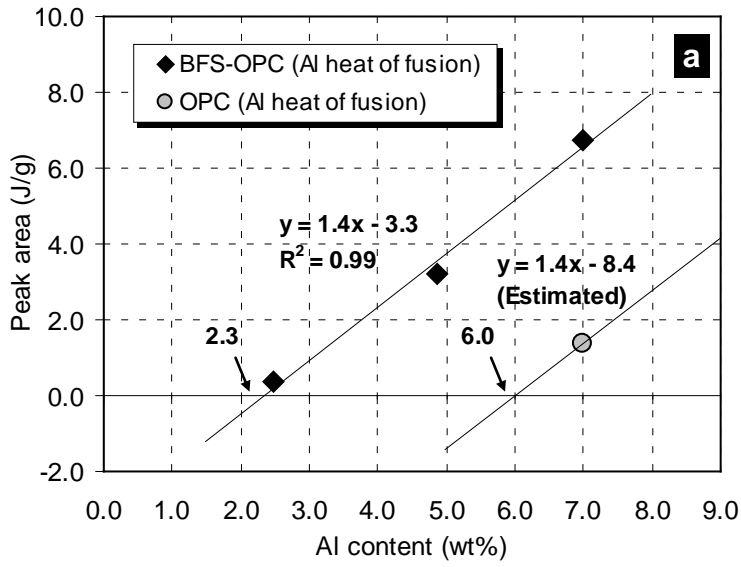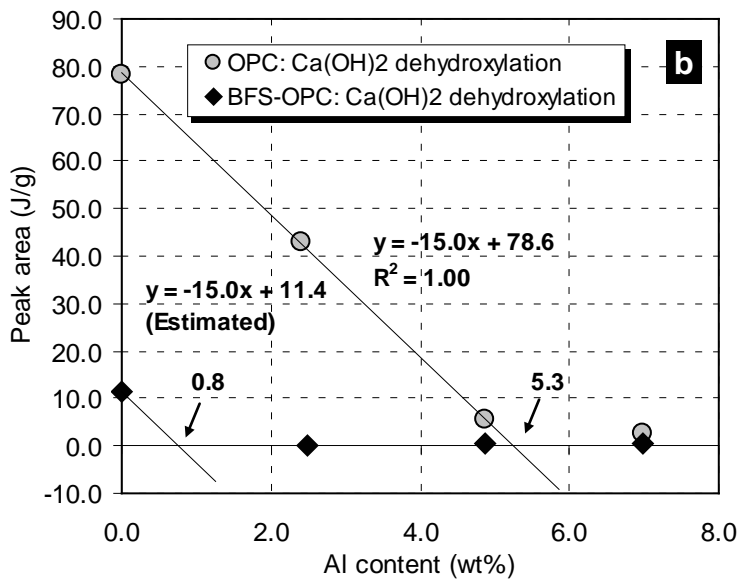
Fig. 7 Peak area in DSC data for OPC and 4:1 BFS-OPC systems with different

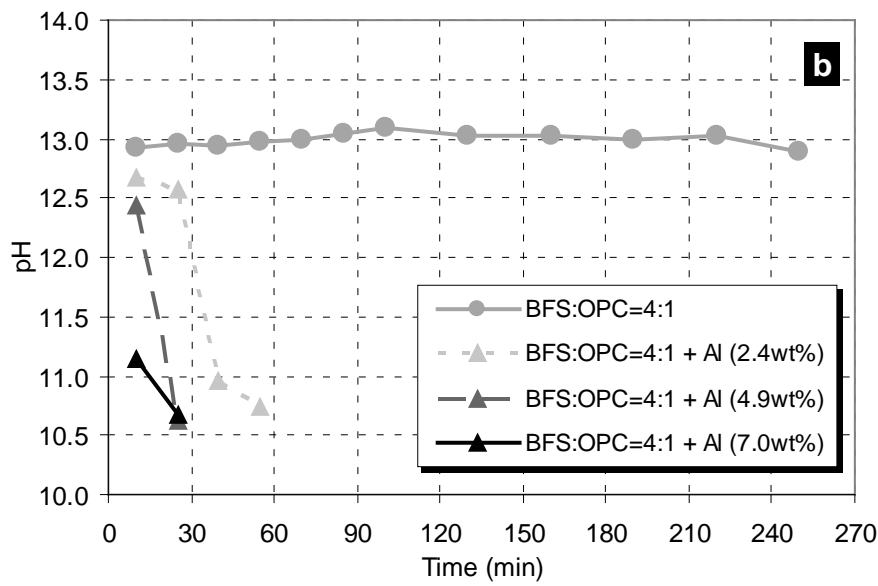amount of aluminium content: (a) endothermic peaks of aluminium fusion in 640-670

^{o}C and (b) endothermic peaks of Ca(OH)$_2$ dehydroxylation in 405-480 ^{o}C.
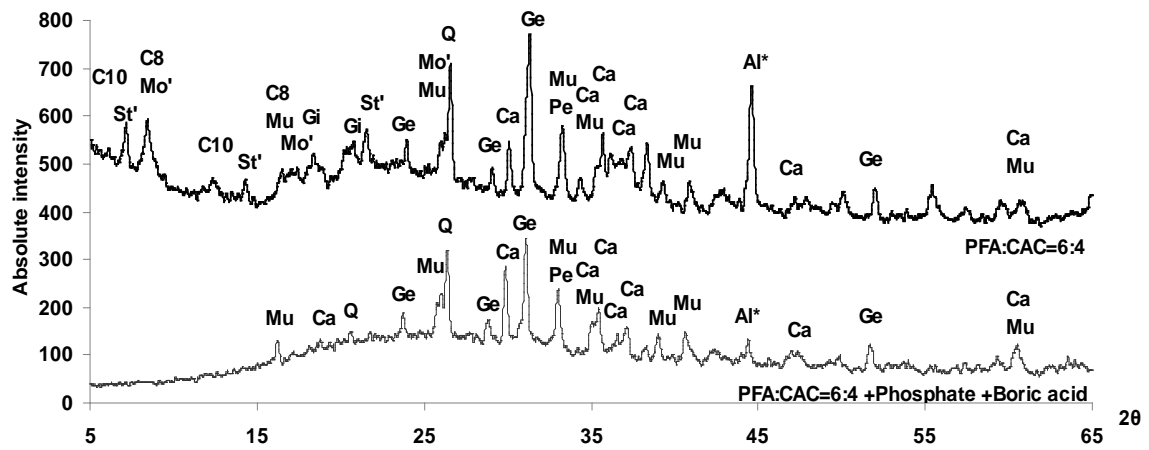
573

574

575

576

577

578 Fig. 8 Change in pH of samples at the initial stage of hydration: (a) for OPC system

579 and (b) for 4:1 BFS-OPC system with different amount of aluminium.

580

581

582

583

584 Fig. 9 XRD pattern of PFA-CAC system with and without addition of sodium

585 polypohosphate and boric acid after 7 days of curing at 20 $^{\circ}$C. Reflection peaks are

586 indexed as: Ca (Monocalcium aluminate), C8 (C_2AH_8), C10 (CAH_{10}), Gi (Gibbsite),

587 Ge (Gehlenite), Mu (Mullite), Mo' (Monosulphate related phase), Pe (Perovskite), Q

588 (Quartz), St' (Strätlingite related phase). Al* is reflection from the Al sample holder.

589

590

591

592
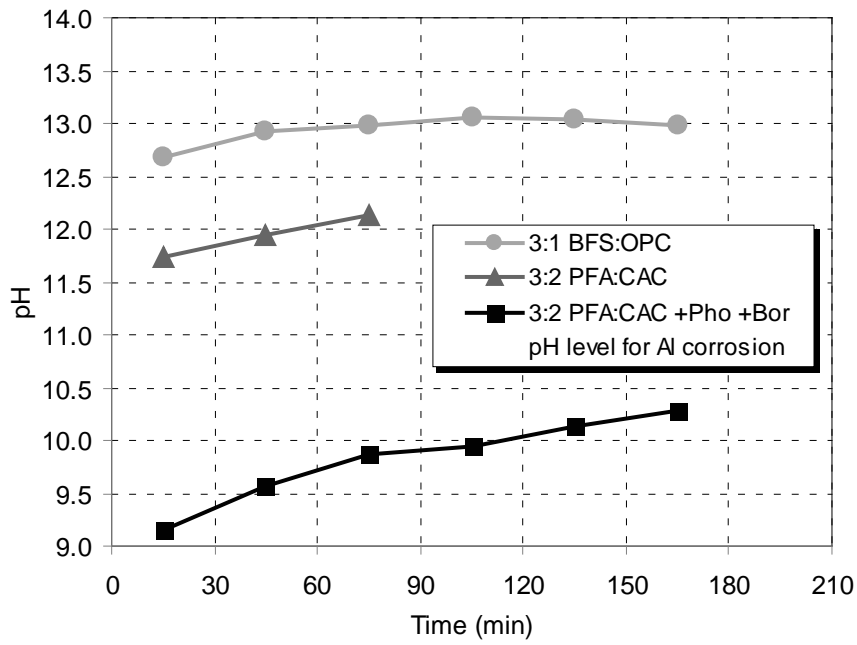
Fig. 10 Change in pH of cement matrices at the initial stage of hydration: CAC-based

systems compared with 3:1 BFS-OPC system.

595